
Physics-Informed Inverse Design of Optical Coatings using a Differentiable Transfer Matrix Method

Utsa Chattopadhyay

Institute for Data Science Foundations
Deutsches Elektronen-Synchrotron DESY
utsa.chattopadhyay@tuhh.de

Florian Carstens

Laser Zentrum Hannover e.V.
f.carstens@lzh.de

Morten Steinecke

Laser Zentrum Hannover e.V.
m.steinecke@lzh.de

Andreas Wienke

Laser Zentrum Hannover e.V.
a.wienke@lzh.de

Ingmar Hartl

Deutsches Elektronen-Synchrotron DESY
ingmar.hartl@desy.de

Nihat Ay

Institute for Data Science Foundations
Santa Fe Institute
nihat.ay@tuhh.de

Christoph M. Heyl

Deutsches Elektronen-Synchrotron DESY
Helmholtz Institute Jena
christoph.heyl@desy.de

Henrik Tünnermann

Deutsches Elektronen-Synchrotron DESY
henrik.tuennermann@desy.de

Abstract

We tackle the challenging inverse design of optical coatings using an artificial intelligence (AI) framework for optical thin-film coating design. Our approach is based on a physics-informed autoencoder with a differentiable physics decoder. Unlike data-driven approaches, our model embeds Maxwell's equations directly through an analytical forward model, enabling end-to-end, gradient-based optimization from target optical properties to physical layer structures, without requiring any prior design examples. We demonstrate our method by designing a complex broadband mirror with a target reflectivity reaching >99% and a precise group delay dispersion of -200 fs^2 over the 940–1120 nm wavelength range. The AI-generated design reaches performance characteristics competitive with state-of-the-art commercial software, demonstrating a powerful and generalizable framework for solving physics-based inverse design problems.

1 Introduction

The inverse design of physical systems represents a fundamental challenge in artificial intelligence and engineering. For complex structures such as optical multilayer coatings, the challenge is to find a physical configuration that yields a desired spectral response. These coatings are indispensable in a wide range of applications, from ultrafast lasers to specialized cameras [1, 2], but their design remains a computationally intensive and expertise-driven task. The design challenge itself is a high-dimensional nonconvex multi-objective optimization problem [3].

Traditional optimization techniques, such as the widely used Needle Algorithm [4, 5], are prone to getting stuck in local minima and often require significant expert guidance to find a suitable

starting point [6]. Although evolutionary algorithms offer a robust alternative [7, 8, 9, 10], their slow convergence makes them inefficient for complex designs [11, 3]. More recently, deep learning methods have shown promise [12, 13, 14, 15], yet these approaches are typically limited to simple single-objective scenarios and Recent work using generative neural networks for anti-reflection coating design provides a crucial step in this direction [16]. However, scaling these models to address complex, multi-objective design problems remains a critical challenge.

We address this gap by proposing a novel physics-informed autoencoder that replaces the standard learnable decoder with a non-parametric, differentiable implementation of the Transfer Matrix Method (TMM), an analytical solution to Maxwell's equations. This enables end-to-end, gradient-based optimization directly guided by physics principles, without relying on any dataset of prior designs. We demonstrate the efficacy of our framework by designing an ultra-broadband dispersive optical multilayer mirror, without incorporating expert input or knowledge about existing designs into the design process. Using only target optical specifications, our framework autonomously derives a solution achieving $>99\%$ reflectivity with a precisely controlled group delay dispersion (GDD) of $-200 \pm 15 \text{ fs}^2$ across a broad spectral range. This result matches the performance of the designs produced by specialized commercial software [17], showcasing the power of our method to solve challenging inverse problems. The work presented here has been discussed by us in detail in [18].

2 Methods

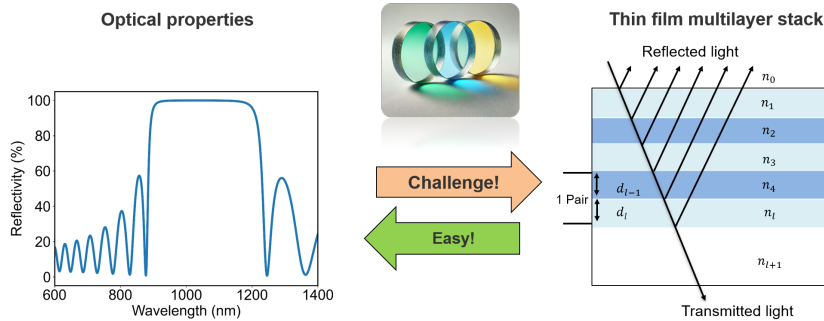


Figure 1: Schematic illustration of the inverse design challenge for optical thin film coatings. The forward problem F (design \rightarrow properties) is computationally straightforward, while the inverse problem (properties \rightarrow design), which this work addresses, represents a major challenge.

The inverse design of optical multilayer coatings requires finding a physical layer structure (layer thicknesses \vec{d} where each vector component represents a single design) that produces the desired set of optical properties x . As illustrated in Fig. 1, this corresponds to finding an approximate right-inverse for the non-bijective forward function F , which is governed by Maxwell's equations. We propose a physics-informed autoencoder framework to solve this ill-posed problem, which, unlike data-driven approaches [19, 6], does not require a dataset of known designs.

2.1 Differentiable Physics-Informed Autoencoder

Our model, illustrated in Fig. 2, consists of an encoder network f_θ and a non-trainable, physics-based decoder F .

Encoder as a Direct Design Predictor: The encoder $f_\theta : \mathcal{X} \rightarrow \mathcal{Z}$ is a neural network with learnable parameters θ . It takes a target set of optical properties $x \in \mathcal{X}$ (e.g. a vector of reflectivity and GDD values) as input. Uniquely, instead of mapping to an abstract latent space, the output of our encoder $z \in \mathcal{Z}$ directly represents the physically interpretable design parameters—the vector of layer thicknesses \vec{d} :

$$z = f_\theta(x) = \vec{d} = (d_1, \dots, d_\ell) \quad (1)$$

where ℓ is the pre-defined number of layers in the stack. This makes the latent space directly interpretable and constrainable.

Decoder as a Differentiable Physics Layer: We replace the standard learnable decoder with a non-trainable, differentiable layer that implements the physical forward model, $F : \mathcal{Z} \rightarrow \mathcal{X}$. This layer is based on the Transfer Matrix Method (TMM) [20], an analytical solution to Maxwell's equations for multilayer films (See Appendix A.1). It takes the predicted layer thicknesses \vec{d} (and fixed material properties \vec{n}) and computes the corresponding optical properties \hat{x} :

$$\hat{x} = F(\vec{d}, \vec{n}) \quad (2)$$

Since the TMM involves a sequence of matrix multiplications, its Jacobian can be computed efficiently via backpropagation through the chain rule, enabling full gradient flow from the output optical spectrum \hat{x} to the input design \vec{d} , and subsequently to the encoder parameters θ . This allows for end-to-end training where the encoder learns to propose physical designs that satisfy the target properties, guided directly by the analytical Transfer Matrix Method (TMM) model.

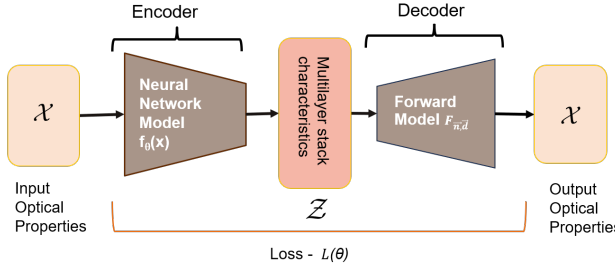


Figure 2: Schematic illustration of the architecture of our model. An encoder f_θ maps target optical properties x , (where $x \rightarrow \mathcal{X}$) to a physically interpretable design $z = \vec{d}$, (where $z \rightarrow \mathcal{Z}$). A non-trainable, differentiable physics layer F (TMM) reconstructs the design to produce \hat{x} .

2.2 Optimization Objective

The network parameters θ are optimized by minimizing a composite loss function $L(\theta)$ that addresses the multi-objective nature of the design problem (e.g., simultaneously optimizing reflectivity and GDD, with α as a weighting hyperparameter):

$$L(\theta) = L_{\text{reflectivity}}(\theta) + \alpha \cdot L_{\text{GDD}}(\theta) \quad (3)$$

The reflectivity loss $L_{\text{reflectivity}}$ is the Mean Squared Error between the target reflectivity spectrum $x^{(i)}$ and the predicted spectrum $\hat{x}^{(i)}$ over m training samples and p wavelength points:

$$L_{\text{reflectivity}}(\theta) = \frac{1}{m} \sum_{i=1}^m \sum_{j=1}^p (x_j^{(i)} - \hat{x}_j^{(i)})^2 \quad (4)$$

To handle physical constraints, the GDD loss L_{GDD} is formulated as a penalty for deviations beyond a specified tolerance t . This selectively penalizes constraint violations:

$$L_{\text{GDD}}(\theta) = \frac{1}{m} \sum_{i=1}^m \sum_{k=1}^p \max(0, |g_k^{(i)} - g_{\text{target}}| - t) \quad (5)$$

where $g_k^{(i)}$ is the predicted GDD for sample i at point k , and g_{target} is the desired GDD. The weighting factor α is annealed during training, initially prioritizing the primary objective (reflectivity) before increasing to enforce the GDD constraints.

Dataset construction: To train our neural network [21], we generate a randomized synthetic dataset of $m = 500$ target optical property data points $x^{(i)}$ by creating a constrained distribution, i.e. a truncated Gaussian distribution centered at a mean of 99.75% with a standard deviation of 0.1% (truncated at 99% and 100%) and with a fixed GDD at -200 fs^2 . This provides structured, relevant targets for training network, a key difference from approaches that start from purely random inputs [16]. It also ensures that the training data represent realistic design targets while avoiding non-physical inputs.

Table 1: Comparison of our AI-generated high-reflectivity mirror with a standard analytical QWOT stack design for the same spectral target. The AI model finds a superior solution.

Design Type	Max. Reflectance	Total Thickness
Analytical QWOT	99.89%	8.9 μm
AI-Generated	99.95%	8.5 μm

3 Results

We evaluated our framework on optical coating design tasks to demonstrate its efficacy and scalability, first on fundamental designs before validating it on a complex, multi-objective inverse problem.

Validation on Fundamental Designs. Our model is first used to demonstrate its ability to generate fundamental single-objective designs. When tasked with creating a high-reflectivity mirror, the framework autonomously produced a design with Quarter-Wave Optical Thickness (QWOT)-like characteristics. As summarized in Table 1, our AI-generated design achieves a slightly higher maximum reflectance (99.95 %) than a standard analytical QWOT stack (99.89 %) while requiring a notably smaller total physical thickness. An increased reflectance as well as a reduction in total thickness of over 4% can be seen as an improvement. A reduced layer thickness leads to a reduced deposition time, lower mechanical stress, and lower material costs in fabrication. This result suggests that our physics-informed approach, which accounts for material absorption, can find superior solutions compared to the standard QWOT stack. Further examples of the framework successfully generating standard edge-pass and narrow-bandpass filters are provided in the Appendix (Fig. 4).

Solving a Complex Multi-Objective Inverse Problem. The primary test of our framework is a demanding multi-objective design challenge: a broadband, high-reflectivity chirped mirror for ultrafast laser applications. The target requires satisfying two simultaneous constraints: achieving $> 99\%$ reflectivity over a broad spectral range (940–1120 nm) while maintaining a tight Group Delay Dispersion (GDD) of $-200 \pm 15 \text{ fs}^2$.

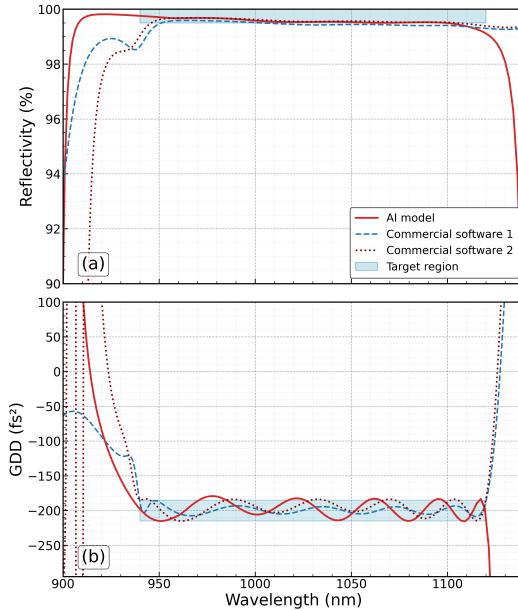


Figure 3: Performance comparison on a multi-objective design task. The reflectivity (a) and GDD (b) of our AI-generated design (solid red) are benchmarked against a design obtained using a commercial optimization software (dashed lines). Similar target and material properties are considered for all three cases.

To benchmark our approach against a robust, established method, we compared our AI-generated design with a design produced by a state-of-the-art commercial software package [17]. Both our

framework and the commercial software were tasked with the same problem under identical constraints, i.e. using the same materials (tantalum pentoxide and fused silica) and identical target specifications. The derived optical properties of both designs are shown in Fig. 3, which results in a total physical thickness of approximately 9 μm each.

4 Conclusion

The results in Fig. 3 demonstrate that our framework autonomously discovers high-quality solutions for a complex, multi-objective inverse problem, achieving performance comparable to specialized commercial software without relying on prior design data. This validates our method’s ability to navigate physically constrained design spaces. In particular, our AI-generated designs exhibit smoother layer thickness profiles than their software-optimized counterparts (see Appendix Fig. 5), an emergent property suggesting a potential for greater manufacturability. The method does not require expert intervention. This opens doors for the automated design of high-performance coatings for ultrafast lasers and other applications. In particular, our approach offers excellent possibilities to enter less explored design parameter spaces and thus offers the potential to find entirely new coating architectures. Future work will extend this framework by incorporating further constraints, such as the laser-induced damage threshold (LIDT) [22], directly into the optimization objective. Future work may also include hybrid approaches that combine our model with data-driven approaches known from classical machine learning that involve training and subsequent inference. This may further enhance the accuracy, speed, and robustness of our design process while offering routes to improved automation and exploitation of unexplored design parameter spaces.

References

- [1] D. Ristau. “OPTICAL COATINGS | Thin Film Optical Coatings”. In: *Encyclopedia of Modern Optics*. Ed. by Robert D. Guenther. Oxford: Elsevier, 2005, pp. 360–369. ISBN: 978-0-12-369395-2. DOI: <https://doi.org/10.1016/B0-12-369395-0/00880-0>. URL: <https://www.sciencedirect.com/science/article/pii/B0123693950008800>.
- [2] P. Zuppella et al. “Optical Coatings: Applications and Metrology”. In: *Engineering Proceedings* 11.1 (2021). ISSN: 2673-4591. DOI: 10.3390/ASEC2021-11137. URL: <https://www.mdpi.com/2673-4591/11/1/50>.
- [3] J. Dai et al. “Efficient multi-objective design method for optical coatings”. In: *Optics and Lasers in Engineering* 184 (2025), p. 108626. ISSN: 0143-8166. DOI: <https://doi.org/10.1016/j.optlaseng.2024.108626>. URL: <https://www.sciencedirect.com/science/article/pii/S0143816624006043>.
- [4] A. V. Tikhonravov, M. K. Trubetskoy, and G. V. DeBell. “Application of the needle optimization technique to the design of optical coatings”. In: *Appl. Opt.* 35.28 (Oct. 1996), pp. 5493–5508. DOI: 10.1364/AO.35.005493. URL: <https://opg.optica.org/ao/abstract.cfm?URI=ao-35-28-5493>.
- [5] A. V. Tikhonravov, M. K. Trubetskoy, and G. W. DeBell. “Optical Coating Design Approaches Based on the Needle Optimization Technique”. In: *Applied Optics* 46.5 (2007), p. 704.
- [6] N. Kaiser. “Old rules useful to the designer of optical coatings.” In: <https://doi.org/10.1002/vipr.200890042> (2008).
- [7] C. Coello et al. *Evolutionary multi-criterion optimization*. Springer, 2005.
- [8] Y. Guo, J. Yaochu, and M. Olhofer. “A multiobjective evolutionary algorithm for finding knee regions using two localized dominance relationships”. In: *IEEE Transactions on Evolutionary Computation* 25.1 (2020), pp. 145–158.
- [9] W. Gao et al. “A gradient-based search method for multi-objective optimization problems”. In: *Information Sciences* 578 (2021), pp. 129–146.
- [10] C. He et al. “A review of surrogate-assisted evolutionary algorithms for expensive optimization problems”. In: *Expert Systems with Applications* 217 (2023), p. 119495.
- [11] A. Piegaro and F. Flory. *Optical thin films and coatings: From materials to applications*. Woodhead Publishing, 2018.
- [12] H. Wang et al. “Automated multi-layer optical design via deep reinforcement learning”. In: *Machine Learning: Science and Technology* 2.2 (Feb. 2021), p. 025013. DOI: 10.1088/2632-2153/abc327. URL: <https://dx.doi.org/10.1088/2632-2153/abc327>.

- [13] H. Youngjoon and David P. Nicholls. “Data-driven design of thin-film optical systems using deep active learning”. In: *Opt. Express* 30.13 (June 2022), pp. 22901–22910. DOI: 10.1364/OE.459295. URL: <https://opg.optica.org/oe/abstract.cfm?URI=oe-30-13-22901>.
- [14] T. Ma, H. Wang, and L. J. Guo. “OptoGPT: a foundation model for inverse design in optical multilayer thin film structures”. In: *Opto-Electronic Advances* 7.7 (2024).
- [15] O. Yesilyurt et al. “Fabrication-conscious neural network based inverse design of single-material variable-index multilayer films”. In: *Nanophotonics* 12.5 (2023), pp. 993–1006.
- [16] J. Jiaqi and Jonathan A. Fan. “Multiobjective and categorical global optimization of photonic structures based on ResNet generative neural networks”. In: *Nanophotonics* 10.1 (2021), pp. 361–369. DOI: doi:10.1515/nanoph-2020-0407. URL: <https://doi.org/10.1515/nanoph-2020-0407>.
- [17] T. Amotchkina et al. “Optical Design: Advanced thin-film software techniques improve design-to-fabrication workflow”. In: *Laser Focus World* 1 (Jan. 2015), pp. 87–90.
- [18] U. Chattopadhyay et al. “Efficient optical coating design using an autoencoder-based neural network model”. In: *Journal of Physics: Photonics* (2025). URL: <http://iopscience.iop.org/article/10.1088/2515-7647/ae1b53>.
- [19] U. Chattopadhyay et al. “Neural Network Method for Dielectric Optical Coating Design”. In: *EPJ Web Conf.* 307 (2024), p. 04057. DOI: 10.1051/epjconf/202430704057. URL: <https://doi.org/10.1051/epjconf/202430704057>.
- [20] L. Alexander et al. “TMM-Fast, a transfer matrix computation package for multilayer thin-film optimization: tutorial”. In: *J. Opt. Soc. Am. A* 39.6 (June 2022), pp. 1007–1013. DOI: 10.1364/JOSAA.450928. URL: <https://opg.optica.org/josaa/abstract.cfm?URI=josaa-39-6-1007>.
- [21] J. Schmidhuber. “Deep learning in neural networks: An overview”. In: *Neural Networks* 61 (Jan. 2015), pp. 85–117. ISSN: 0893-6080. DOI: 10.1016/j.neunet.2014.09.003. URL: <http://dx.doi.org/10.1016/j.neunet.2014.09.003>.
- [22] S. Papernov. *Laser-induced damage in optical materials*. Ed. by D. Ristau. ‘CRC Press’, Nov. 2014, pp. 25–73. ISBN: 978-1-4398-7216-1.
- [23] D. Bank, N. Koenigstein, and R. Giryes. “Autoencoders”. In: *Machine Learning for Data Science Handbook: Data Mining and Knowledge Discovery Handbook*. Ed. by L. Rokach, O. Maimon, and E. Shmueli. Cham: Springer International Publishing, 2023, pp. 353–374. ISBN: 978-3-031-24628-9. DOI: 10.1007/978-3-031-24628-9_16. URL: https://doi.org/10.1007/978-3-031-24628-9_16.
- [24] M. Umberto. *An Introduction to Autoencoders*. 2022. arXiv: 2201.03898 [cs.LG]. URL: <https://arxiv.org/abs/2201.03898>.
- [25] T. Mackay and A. Lakhtakia. “The Transfer-Matrix Method in Electromagnetics and Optics”. In: *Synthesis Lectures on Electromagnetics* 1 (Apr. 2020), pp. 1–126. DOI: 10.2200/S00993ED1V01Y202002EMA001.

A Technical Appendices and Supplementary Material

A.1 TMM

In a conventional autoencoder architecture [23, 24] a trained neural network is used as a decoder, mapping the latent space to an output. In contrast, our approach replaces the decoding step with a physics-based forward model. This model, based on the well-known transfer matrix method (TMM) [20, 25], analytically calculates linear light propagation through multiple interfaces, ensuring the basic principles defined by Maxwell’s equations [3]. The TMM uses an index jump matrix, which depends on the refractive indices of adjacent layers and the angle of incidence. The interaction at interfaces and within layers is captured by propagation matrices (T_P) and interface matrices (T), leading to a total transformation matrix which can be expressed as:

$$\mathbf{T}_{total}(\vec{n}, \vec{d}, \phi) = \mathbf{T}(n_0, n_1) \cdot \mathbf{T}_P(n_1, d_1, \phi) \dots \mathbf{T}(n_\ell, n_{\ell+1}) \cdot \mathbf{T}_P(n_{\ell+1}, d_{\ell+1}, \phi) \quad (6)$$

Both the propagation and interface matrices depend on the refractive index (\vec{n}), the thickness of the layer (\vec{d}), and the incident angle of light (ϕ). This approach ensures that the neural network does not

need to learn the underlying physics of light propagation from existing data sets. Instead, the forward model ($F_{\vec{n}, \vec{d}}$) directly enforces physical consistency, as indicated in fig 2.

A.2 QWOT stack

The framework's adaptability to diverse design targets is demonstrated in Fig. 4(c) and (d). Fig 4(c) shows an AI-generated edge filter designed to transition from high transmission to high reflection around a 600 nm cutoff. The resulting design successfully achieves this, reaching a reflectivity of >99.9% in the stopband (above 700 nm) while maintaining high transmission in the passband (450-600 nm). Similarly, the narrow bandpass filter shown in Fig. 4(d) effectively isolates a high-transmission window centered at 720 nm while strongly rejecting the surrounding spectral regions.

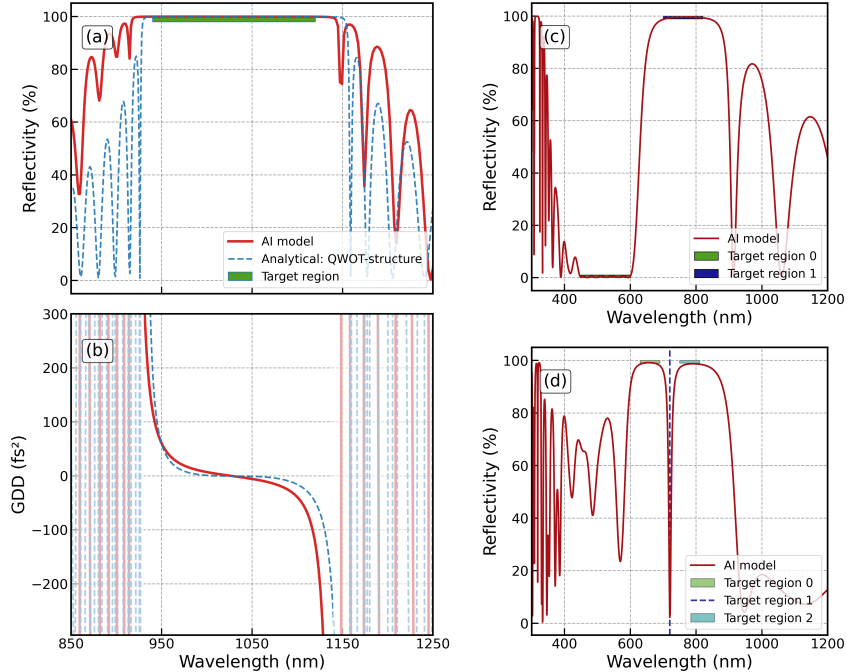


Figure 4: Validation of the AI framework using basic optical coating designs. **(a)** AI-generated high-reflectance broad-bandwidth mirror and an analytically calculated Quarter-Wave Optical Thickness (QWOT) stack. **(b)** Corresponding Group Delay Dispersion (GDD) for the designs displayed in (a). **(c)** AI-generated edge pass filter, showing a gradual transition from minimum reflectance (passband) to maximum reflectance (stopband). **(d)** AI-generated narrow bandpass filter featuring high transmission at 720 nm and high reflectance in the surrounding spectral regions.

A.3 Layer stack

Fig 5 provides a detailed comparison of the physical layer stack designs corresponding to the optical performance shown in the main text (Fig. 3). The figure displays the individual layer thicknesses for three designs: **(a)** the design generated by our AI framework, **(b)** the initial design of the commercial software design 1 and **(c)** commercial software design 2.

As discussed in the main text, a notable difference is apparent in the layer thickness profiles. The AI-generated design exhibits a smoother distribution of layer thicknesses. In contrast, the designs produced by the commercial software, particularly the expert-tuned version (c), feature more extreme thickness variations, including a significant number of very thin layers (e.g., sub-nanometer). Such features can present challenges for certain physical deposition processes, suggesting that our AI framework may inherently find solutions in more manufacturable regions of the design space.

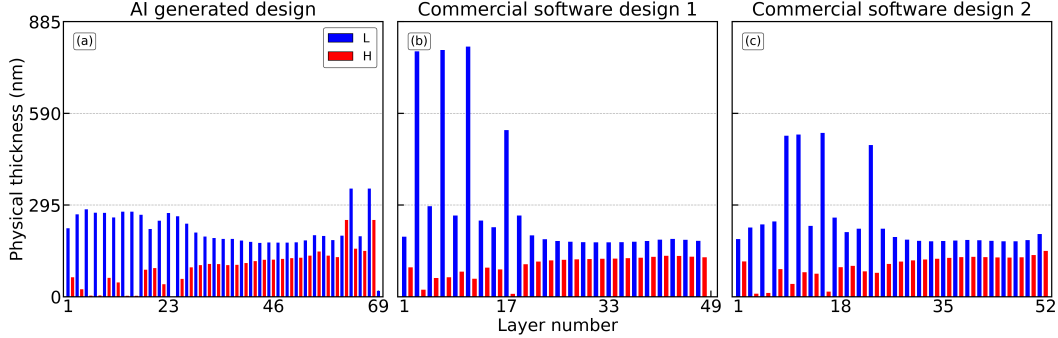


Figure 5: Comparison of the layer thickness distributions for the broadband chirped mirror presented in fig 3: (a) AI-optimized design, (b) Commercial software design 1, and (c) Commercial software design 2. The lower index materials are denoted as L and the higher index material as H.

A.4 Training Details and Hyperparameters

This section provides additional details regarding the training procedure and the hyperparameters used for the results presented in the main text. For all designs, layer 0 is the incident layer, whereas the layer after the last layer is the substrate material.

A.4.1 Hyperparameter Settings

The neural network encoder and the training process were configured with the hyperparameters listed in Table 2. These values were determined through a combination of common practices in deep learning and empirical tuning for our specific optical design problem.

Table 2: Key hyperparameters for the encoder network and training process.

Hyperparameter	Value
<i>Encoder Architecture</i>	
Hidden Layers	3
Neurons per Layer	64, 64, 64, [Number of Layers in Stack]
Activation Function	ReLU (hidden), Sigmoid (output)
Output Layer Scaling	Temperature Scaling
<i>Training Parameters</i>	
Optimizer	Adam
Learning Rate	5×10^{-4}
Batch Size	32
Number of Epochs	1200

A.4.2 Training Convergence

The training of the model was monitored by observing the composite loss function over the training epochs. A representative training loss curve for the broadband chirped mirror design is shown in Fig 6. The curve demonstrates stable convergence, with a rapid initial decrease in loss as the model learns the primary reflectivity objective, followed by a slower, steady refinement as it balances both reflectivity and the GDD constraints. Training was typically done on a single NVIDIA RTX 4090 GPU.

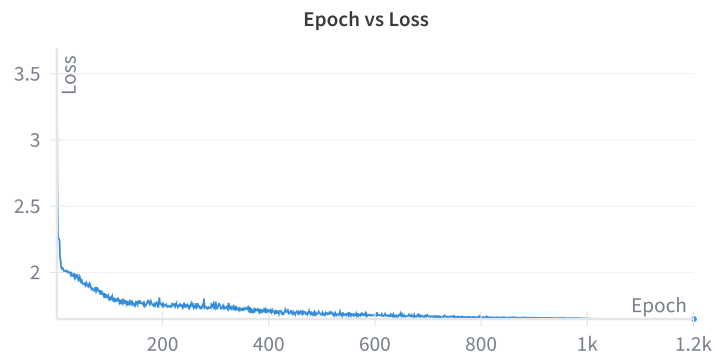


Figure 6: A representative training loss curve for the multi-objective optimization of the broadband chirped mirror. The y-axis shows the total loss (log scale), and the x-axis shows the training epochs. The smooth convergence indicates a stable learning process.